Low V_{pp}, ultralow-energy, compact, high-speed silicon electro-optic modulator

Po Dong[1]*, Shirong Liao[1], Dazeng Feng[1], Hong Liang[1], Dawei Zheng[1], Roshanak Shafiiha[1], Cheng-Chih Kung[1], Wei Qian[1], Guoliang Li[2], Xuezhe Zheng[2], Ashok V. Krishnamoorthy[2], and Mehdi Asghari[1]

[1]*Kotura Inc., 2630 Corporate Place, Monterey Park, CA, 91754, U.S.A.*
[2]*Sun Microsystems, Physical Sciences Center, San Diego, CA 92121, U.S.A.*
**pdong@kotura.com*

Abstract: We present a high-speed silicon optical modulator with a low V_{pp} (peak-to-peak driving voltage) and ultralow energy consumption based on a microring resonator, with the refractive index modulation achieved by electric-field-induced carrier depletion in a reverse-biased lateral pn diode embedded in the ring structure. With a V_{pp} of 2 V, we demonstrate a silicon modulator with a 3 dB bandwidth of 11 GHz, a modulation depth of 6.5 dB together with an insertion loss of 2 dB, ultralow energy consumption of 50 fJ per bit, and a small device active area of ~1000 μm^2.

OCIS codes: (230.3120) Integrated optics devices; (250.7360) Waveguide modulators; (250.5300) Photonic integrated circuits; (200.4650) Optical interconnects.

References and links

1. R. A. Soref, "The past, present and future of silicon photonics," IEEE J. Sel. Top. Quantum Electron. **12**(6), 1678–1687 (2006).
2. L. C. Kimerling, *et al*., "Electronic–photonic integrated circuits on the CMOS platform," Proc. SPIE **6125**, 6–15 (2006).
3. D. A. B. Miller, "Optical interconnects to silicon," IEEE J. Sel. Top. Quantum Electron. **6**(6), 1312–1317 (2000).
4. B. Jalali, M. Paniccia, and G. Reed, "Silicon photonics," IEEE Microw. Mag. **7**(3), 58–68 (2006).
5. A. V. Krishnamoorthy, R. Ho, X. Zheng, H. Schwetman, J. Lexau, P. Koka, G. Li, I. Shubin, and J. E. Cunningham, "Computer systems based on silicon photonic interconnects," Proc. IEEE **97**, 1337–1361 (2009).
6. A. Liu, R. Jones, L. Liao, D. Samara-Rubio, D. Rubin, O. Cohen, R. Nicolaescu, and M. Paniccia, "A high-speed silicon optical modulator based on a metal-oxide-semiconductor capacitor," Nature **427**(6975), 615–618 (2004).
7. Q. Xu, B. Schmidt, S. Pradhan, and M. Lipson, "Micrometre-scale silicon electro-optic modulator," Nature **435**(7040), 325–327 (2005).
8. Q. Xu, S. Manipatruni, B. Schmidt, J. Shakya, and M. Lipson, "12.5 Gbit/s carrier-injection-based silicon micro-ring silicon modulators," Opt. Express **15**(2), 430–436 (2007).
9. S. Manipatruni, Q. Xu, B. Schmidt, J. Shakya, and M. Lipson, "High speed carrier injection 18 Gb/s silicon micro-ring electro-optic modulator," in *Proceedings of LEOS 2007* (IEEE 2007), pp. 537–538.
10. S. Manipatruni, L. Chen, and M. Lipson, "50 Gbit/s wavelength division multiplexing using silicon microring modulators," in *Proceedings of 6th IEEE International Conference on Group IV Photonics* (IEEE 2009), pp. 244–246.
11. W. M. Green, M. J. Rooks, L. Sekaric, and Y. A. Vlasov, "Ultra-compact, low RF power, 10 Gb/s silicon Mach-Zehnder modulator," Opt. Express **15**(25), 17106–17113 (2007).
12. A. Liu, L. Liao, D. Rubin, H. Nguyen, B. Ciftcioglu, Y. Chetrit, N. Izhaky, and M. Paniccia, "High-speed optical modulation based on carrier depletion in a silicon waveguide," Opt. Express **15**(2), 660–668 (2007).
13. L. Liao, A. Liu, D. Rubin, J. Basak, Y. Chetrit, H. Nguyen, R. Cohen, N. Izhaky, and M. Paniccia, "40 Gbit/s silicon optical modulator for high speed applications," Electron. Lett. **43**(22), 1196–1197 (2007).
14. A. Liu, *et al*., "200 Gbps photonic integrated chip on silicon platform," in *Proceedings of 5th IEEE International Conference on Group IV Photonics* (IEEE 2008), pp. 368–370.
15. S. J. Spector, *et al*., "High-speed silicon electro-optical modulator that can be operated in carrier depletion or carrier injection mode," in *the Proceedings of the Conference on Lasers and Electro-Optics* (IEEE 2008), paper CHF4.
16. D. M. Gill, *et al*., "CMOS compatible Si-Ring Assisted Mach-Zehnder interferometer with internal bandwidth equalization," in *Proceedings of 6th IEEE International Conference on Group IV Photonics* (IEEE 2009), paper PD 1.2.
17. D. W. Zheng, D. Z. Feng, G. Gutierrez, and T. Smith, "Design of a 10 GHz silicon modulator based on a 0.25 µm CMOS process - a silicon photonic approach," Proceedings of SPIE **6125**, pp. 61250E.1–61250E.10 (2006).

#117108 - $15.00 USD Received 11 Sep 2009; revised 12 Nov 2009; accepted 17 Nov 2009; published 24 Nov 2009

18. F. Y. Gardes, G. T. Reed, N. G. Emerson, and C. E. Png, "A sub-micron depletion-type photonic modulator in silicon on insulator," Opt. Express **13**(22), 8845–8853 (2005).
19. R. A. Soref, and B. R. Bennett, "Electrooptical effects in silicon," IEEE J. Quantum Electron. **23**(1), 123–129 (1987).
20. J. F. Liu, D. Pan, S. Jongthammanurak, K. Wada, L. C. Kimerling, and J. Michel, "Design of monolithically integrated GeSi electro-absorption modulators and photodetectors on a SOI platform," Opt. Express **15**(2), 623–628 (2007).
21. J. F. Liu, M. Beals, A. Pomerene, S. Bernardis, R. Sun, J. Cheng, L. C. Kimerling, and J. Michel, "Waveguide-integrated, ultralow-energy GeSi electro-absorption modulators," Nat. Photonics **2**(7), 433–437 (2008).
22. M. R. Watts, D. C. Trotter, R. W. Young, and A. L. Lentine, "Ultralow power silicon microdisk modulators and switches," in *Proceedings of 5th IEEE International Conference on Group IV Photonics* (IEEE 2008), pp. 4 - 6.
23. R. F. Pierret, *Semiconductor device Fundamentals* (Addison-Wesley, 1996).
24. M. Shur, *Physics of semiconductor devices* (Prentice Hall, 1990).
25. J. B. You, M. Park, J. W. Park, and G. Kim, "12.5 Gbps optical modulation of silicon racetrack resonator based on carrier-depletion in asymmetric p-n diode," Opt. Express **16**(22), 18340–18344 (2008).
26. P. Dong et al., Kotura Inc, 2630 Corporate Place, Monterey Park, CA, 91754, USA, are preparing a manuscript to be called "Low power multiplexing devices based on silicon microring resonator."
27. N. Sherwood-Droz, H. Wang, L. Chen, B. G. Lee, A. Biberman, K. Bergman, and M. Lipson, "Optical 4x4 hitless slicon router for optical networks-on-chip (NoC)," Opt. Express **16**(20), 15915–15922 (2008).

Optical interconnect technology is perceived as a key solution to solving major performance limitations in high performance computing caused by bus bandwidth bottleneck, latency and power consumption issues [1–4]. While these issues have caused the clock frequencies to saturate at a few GHz, the use of multi-thread and multi-core processor technologies have enabled processor performance to scale forward. However, the parallelism resulting from such architectures and the resulting aggregate bandwidth, place stringent requirements on the power and footprint of the interconnecting technology. It is widely accepted that Si photonics, due to its electronics integration capability, proven manufacturing record and price volume curve, will form the platform of choice for this interconnect technology [5]. A key component to enabling this is a high-speed, efficient modulator requiring a low drive voltage and a small footprint. Although significant progress has been made in this area [6–18], previously demonstrated silicon modulators do not fully satisfy these requirements for on-chip applications. Here, we present a high-speed silicon optical modulator that is the closest to date of any reported device to demonstrating the combined system level performance requirements placed on such a device.

On chip applications of silicon modulators require excellent electrical and optical performance in terms of speed, power/energy consumption, dynamic voltage swing, modulation depth, insertion loss, and device size. Particularly, a compact silicon modulator with a low V_{pp} and low energy for which optical performance is not sacrificed is highly desired [5]. In recent years, high-speed waveguide based silicon modulators have been developed using the plasma dispersion effect [19], where the refraction index of silicon is changed by injecting/removing free carriers. The demonstrated modulators were based on either a MOS capacitor [6], a forward-biased p-i-n diode [7–11], or a reverse-biased pn junction [12–18]. Due to the weak index change induced by this effect, previously demonstrated silicon modulators suffer from either high power consumption and high V_{pp}, or high insertion loss.

Table 1 summarizes the device performance for various silicon-integrated modulators including a reversed-biased Mach-Zehnder interferometer (MZI) modulator [12], a forward-biased MZI modulator [11], a forward-biased p-i-n based microring modulator [8–10], a GeSi electro-absorption modulator [20,21], a reversed-biased disk modulator [22], and the device presented in this work. MZI based modulators usually exhibit a large footprint, have a energy consumption greater than 5 pJ per bit, and require a large V_{pp} of 6-8 V. Microring based modulators can dramatically reduce the power consumption by taking advantage of strong light confinement in the resonator, however, the demonstrated forward-biased p-i-n modulator requires a V_{pp} of ~3.5 V and a complex pre-emphasis driving signal to achieve high speed operation [7–10]. Recently demonstrated SiGe electro-absorption modulators integrated with Si waveguides [20,21] exhibit low power consumption, but suffer from large insertion loss due to residual material absorption and fabrication complexity due to GeSi growth. Another

#117108 - $15.00 USD Received 11 Sep 2009; revised 12 Nov 2009; accepted 17 Nov 2009; published 24 Nov 2009

modulator example which has ultralow energy is a silicon disk modulator using reverse-biased vertical pn junction reported in ref. 22. This disk device exhibits a V_{pp} of 3.5 V and power consumption of 85 fJ/bit, and may suffer from high-order resonance associated with the disk cavity structure, which limits possible wavelength channels if wavelength division multiplexing is used. In comparison, the reverse-biased microring modulator in this work demonstrates a 3dB bandwidth of 11 GHz with a low V_{pp} of 2 V and ultralow energy consumption of 50 fJ per bit without suffering from optical performance.

Table 1. Comparison of previously demonstrated silicon-integrated modulators and the reverse-biased ring modulator presented in this work.

	Reverse-biased MZI[a]	Forward-biased MZI[b]	Forward-biased ring[c]	GeSi EA modulator[d]	Reverse-biased disk[e]	Reverse-biased ring[f]
Device footprint (μm²)	~1 x 10^4	~1 x 10^3	~1 x10^2	~2 x 10^2	~20	~1 x 10^3
V_{pp} to achieve high speed operation (V)	6.5	7.6[#]	3.5[#]	3.0	3.5	2.0
Speed achieved[*]	~20 GHz	10 Gbps	>12.5 Gbps	1.2 GHz	10 Gbps	11 GHz
Energy per bit (fJ/bit)	~3 x10^4	5 x 10^3	~300	50	85	50
Modulation depth & insertion loss (dB) [†]	>20 & ~7	6-10 & 12	>10 & <0.5	8 & ~5	8 & ~1.5	6.5 & 2
Working spectrum width (nm)	>20	-	~0.1	~14	~0.1	~0.1

[a] Taken from ref. 12; [b] taken from ref. 11; [c] taken from refs. 8-10; [d] taken from ref. 21; [e] taken from 22; [f] taken from this work.
[*] The unit of speed may be GHz (which represents devices' 3 dB bandwidth) or Gbps (which comes from the speed of NRZ modulation).
[†] Modulation depth is the power ratio between on/off status under d.c. condition, and insertion loss is the power loss at on status under d.c. condition.
[#] V_{pp} after pre-emphasis.

The modulator reported here consists of a ring resonator coupled to a neighboring bus waveguide [Fig. 1(a)]. The bus and ring waveguides have a width of 0.5 μm, a height of 0.25 μm and a slab height of 50 nm. Such waveguide geometry enables very tight waveguide bend radii, down to a few microns. The optical resonance condition is satisfied when the circumference of the ring corresponds to an integer multiple of the guided light wavelength. The transmission of an optical signal at the resonant wavelength can be dramatically reduced, and the extinction ratio between on/off resonance can be greatly enhanced under the critical condition where the power coupling between the ring and the waveguide equals the round trip loss of the ring. Tuning the effective index of the ring waveguide modifies the resonant wavelength which induces a strong modulation of the transmitted signal. To achieve this, we design a lateral pn diode along the ring waveguide. For a reverse-biased pn junction, a high electrical field is built up across the junction and sweeps out the free electrons and holes in the depletion region [23,24]. The depletion width depends on the bias voltage and the doping concentrations [23,24]. Altering the bias voltage modifies the depletion width and hence the effective index of the ring waveguide through the plasma dispersion effect [19]. In general, increasing the doping concentration increases the index change with a fixed bias voltage [12], however, it would also increase the optical loss of the ring waveguides. By optimizing the overlap between the optical mode and the depletion region, we designed an asymmetric pn junction with a p doping concentration of $5x10^{17}$ cm^{-3} and an n doping concentration of $1x10^{18}$ cm^{-3}. The pn junction position is set at 50 nm offset from the mode centre because hole concentration changes induce a larger index change than electron concentration changes [19]. In order to ensure a good ohmic contact between silicon and metal, heavy doped p + + and n + + regions with doping concentrations of ~$1x10^{20}$ cm^{-3} are utilized at the metal to silicon interface. In addition, the metal contacts are positioned over 250 nm silicon regions

#117108 - $15.00 USD Received 11 Sep 2009; revised 12 Nov 2009; accepted 17 Nov 2009; published 24 Nov 2009

rather than 50 nm slab areas, as shown in Fig. 1(b). This reduces possible metal-induced optical loss due to the proximity of the metal to the waveguide.

The device was fabricated on a silicon-on-insulator (SOI) platform with a 3-μm-thick buried oxide. Following waveguide trench etching, multiple lithography steps were used to define various doping areas. High-energy ion implantation and rapid thermal annealing defined the pn diode and the heavy doping regions. Afterwards, titanium silicides were formed on the contact areas to reduce contact resistivity. It is critical to achieve low contact resistance so that the device speed is not limited by resistance-capacitance time (RC time) [23,24]. We deposited oxide as a top cladding layer to protect the waveguide and ring, and nitride as a passivation layer to protect metals. Figure 1(a) shows the top-view scanning electron microscopy (SEM) image of a fully fabricated ring modulator with a radius of 15 μm and a ring-bus gap of 180 nm.

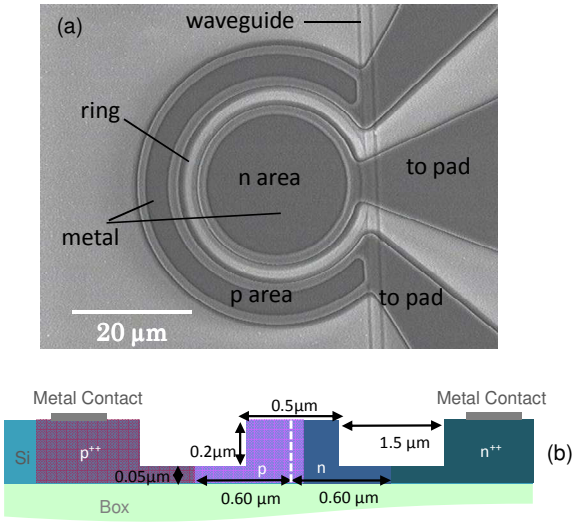

Fig. 1. SEM image of the fabricated device and schematic cross section of the ring waveguide. a, Top-view SEM image of the fully fabricated device The ring and waveguide are clad by a 1.2-μm-thick oxide, followed by contact area etch. The metal covers the contact area and links to pad areas. b, schematic cross section of the ring waveguide. The white line indicates the middle line of the waveguide.

Transmission spectra under different bias voltages demonstrate a large resonance shift which enables high modulation depth with a low V_{pp}. Figure 2(a) presents the transmission spectra with bias voltages of 0V, −1V and −2V, respectively. The on/off extinction ratio of the ring resonance exceeds 15 dB, demonstrating the ring is operated almost under the critical coupling condition. The quality factor of the ring resonator is estimated at ~14500. The resonance shift per unit voltage is 18 pm/V. This value is significantly larger than that of a similar racetrack resonator silicon modulator (2.3 pm/V) using lateral reverse biased pn junction [25]. Another figure of merit for modulation efficiency usually used in MZI modulators, $V \cdot L_\pi$ (L_π is the device length needed to achieve a π phase shift) is ~1.5 V·cm for this device. If we use V_{pp} = 2 V to drive the modulator, the on/off modulation ratio and insertion loss can be obtained from the spectral measurement at 0 V and −2 V. One can see that, from Fig. 2(b), there are two modulation ratio peaks, which arise due to two different resonant wavelengths at 0 V and −2 V respectively. This modulator can operate at either of these peaks. At a wavelength of 1551.84 nm, we achieve a modulation depth of 6.5 dB and an insertion loss of 2 dB, which are values comparable to typical modulator performance requirements seen in the optical industry. If we can tolerate more insertion loss (~3 dB), a modulation depth of ~12 dB is achievable.

#117108 - $15.00 USD Received 11 Sep 2009; revised 12 Nov 2009; accepted 17 Nov 2009; published 24 Nov 2009

Ultra-low energy consumption for high-speed modulation relies on low device capacitance. For a reverse biased pn diode, the energy consumption for dynamic modulation is mainly determined by the transient energy consumption during the on/off transitions since the DC current is extremely low [< 1 nA in the device shown in Fig. 1(a)]. For non-return-to-zero (NRZ) modulation, the energy consumption per bit can be expressed as

$$\text{Energy/bit} = ¼\, CV_{pp}^2 \tag{1}$$

where C is the device capacitance (the factor 4 is due to the fact that the 0-1 transition only happens with a probability of 0.25 for all bit sequences [22]). Considering an experimentally measured junction capacitance of ~50 fF for our device and a V_{pp} of 2 V, we can obtain the energy consumption per bit as 50 fJ/bit. This can be further reduced by scaling down the ring radius to a few microns.

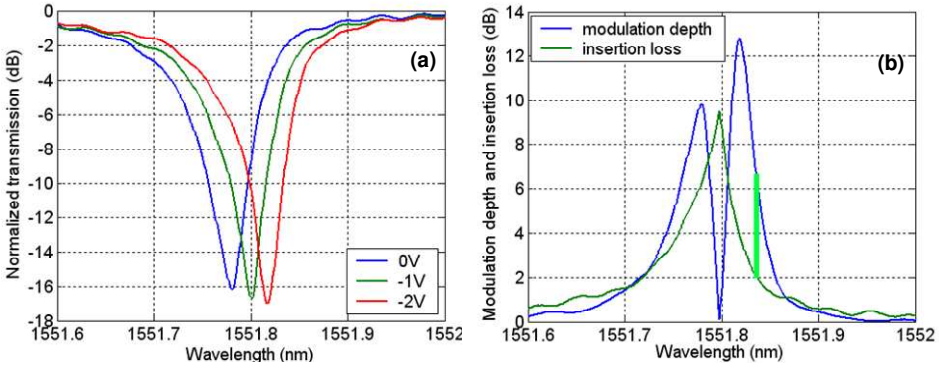

Fig. 2. DC performance of the reverse biased ring modulator. a, Transmission spectra of the ring resonator at bias voltages of 0 V, −1 V, and −2 V respectively. b, Modulation depth and insertion loss with a V_{pp} = 2 V (0 V to −2 V) as a function of wavelength. The green bar indicated the wavelength region for a 6.5 dB modulation depth and a 2 dB insertion loss.

The device 3 dB modulation bandwidth is determined by the RC time and the photon lifetime, as expressed by

$$\frac{1}{f_{3dB}^2} = (2\pi\tau)^2 + (2\pi RC)^2 \tag{2}$$

where $\tau = \dfrac{\lambda Q}{2\pi c}$ is the cavity photon lifetime (c is the light speed in vacuum and Q is the quality factor). The contact resistance of our device is measured as 55 ohm. The RC time is therefore ~3 ps, which results in a RC limited 3dB bandwidth larger than 50 GHz (This calculation does not include external impedances such as those from RF cables or probes in practical experimental setups). Therefore, in our case the device speed is mainly limited by the cavity photon lifetime required to built up and release the energy from the ring resonator. From the measured quality factor, the 3 dB bandwidth is calculated to be ~13 GHz from Eq. (2).

We measured the small signal electro-optical (EO) response of the modulator in the frequency range of 50 MHz to 20 GHz with an input RF power of −5 dBm and a bias voltage of −1V. Continuous-wave (CW) light with a wavelength −0.05 nm offset from the ring resonance is coupled to the device, and the RF signal from a network analyzer is applied on the device through a high-speed probe which has a 50 ohm terminator to minimize the RF reflection due to the impedance mismatch between RF cables and the modulator. The modulated optical signal, amplified by an erbium-doped fiber amplifier (EDFA), is measured

#117108 - $15.00 USD Received 11 Sep 2009; revised 12 Nov 2009; accepted 17 Nov 2009; published 24 Nov 2009

by a high-speed optical detector, and the electrical output is sent to the network analyzer. The 3 dB bandwidth of our device is observed to be 11 GHz, as shown in Fig. 3. The measured bandwidth is close to the calculated value from Eq. (2) and should enable ~14 Gbps operation. There is no frequency roll-off up to 6 GHz, indicating that the device can achieve high modulation depth up to 6 GHz as in the d.c. case. Figure 4 shows eye diagrams for high-speed modulation. The modulator is driven by an NRZ PRBS 2^{23}-1 signal with a V_{pp} of 2V and a d.c. bias of −1V. The eye diagrams were measured using a high-speed oscilloscope equipped with an optical detector. The measured eye diagrams exhibit clear eye openings for both 5 Gbps and 10 Gbps, with an extinction ratio of ~8 dB (we chose a wavelength near resonance). Further improvement of modulation speed up to 20 Gbps can be achieved by optimizing the doping profile of the pn junction and decreasing the ring waveguide scattering loss.

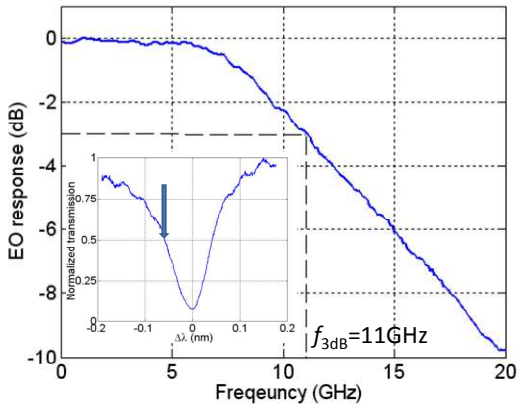

Fig. 3. Dynamic EO response of the device. The main panel shows the EO response in the frequency range of 50 MHz to 20 GHz with a small signal drive. The 3 dB bandwidth is determined as 11GHz and no frequency roll-off is observed up to 6 GHz. The transmission spectrum (inset) is taken during the EO response measurement. We chose a wavelength for this measurement such that that the normalized transmitted power is ~0.5 (the most linear regime in the ring resonance).

Table 1 indicates that the main challenge to the use of ring modulators is their ultra narrow operation spectrum bandwidth (~0.1 nm in this case) without any resonance tuning elements. In addition, any fabrication error can shift the resonant wavelength of a ring resonator. What negates this major disadvantage is the large thermo-optic coefficient (~1.86×10^{-4} /°C) of Si and the resulting high thermal tuning efficiency achievable for on-chip heaters. We anticipate that this together with a well designed waveguide structure and heater elements should enable tuning energies in the few mW range for a few nm wavelength shift for a ring resonator modulator of a few micron ring radius [26,27]. If the ring modulator is operated at 20 Gbps, the whole energy consumption per bit would be less than 500 fJ per bit, which may be acceptable for applications in macrochip and off-chip communications [5]. Including this additional power consumption, the ring modulator still requires much less power than MZI modulators.

#117108 - $15.00 USD Received 11 Sep 2009; revised 12 Nov 2009; accepted 17 Nov 2009; published 24 Nov 2009

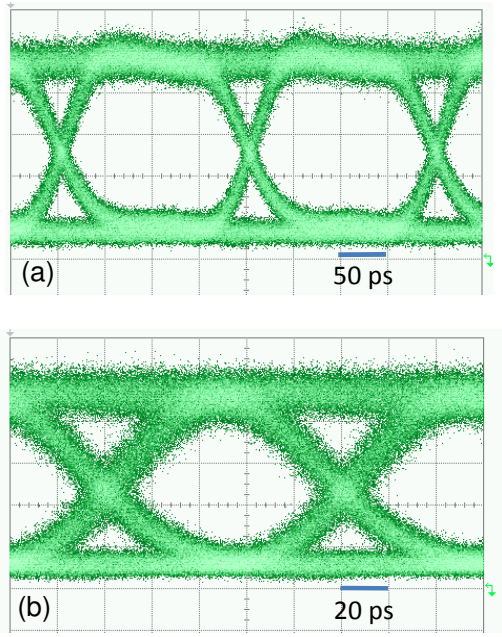

Fig. 4. High-speed modulation of the device. The eye diagrams are measured with NRZ signal (PRBS $2^{23}-1$, $V_{pp} = 2$ V, $V_{dc} = -1$ V) at 5 Gbps (a) and 10 Gbps (b).

In conclusion, a compact (~1000 μm^2), low loss (2 dB), and high-speed (11 GHz) silicon electro-optic modulator with a very low V_{pp} (2V) and ultralow energy consumption (50 fJ/bit) has been demonstrated. This modulator consists of a ring resonator as an optical platform and realizes index modulation by using a reversed-biased lateral pn diode embedded in the ring. The low insertion loss is achieved because there are no carrier-induced losses in the bus waveguide. This has the added advantage of enabling further optimization of the junction doping profile to achieve improved modulation efficiency while maintaining a low V_{pp}. The device structure is fully CMOS compatible as only standard doping and etching are utilized. In addition, the ring radius can be scaled down to a few microns which would reduce the energy consumption and device area further. This device can serve as one of the most critical components in large-scale electronic-photonic integration on silicon.

Acknowledgements

The authors acknowledge funding of this work by DARPA MTO office under UNIC program supervised by Jagdeep Shah (contract agreement with SUN Microsystems HR0011-08-9-0001). The authors greatly acknowledge Dr. Joan Fong and Dr. B. J. Luff from Kotura Inc. for their work in fabricating of the device and revising the manuscript, and Dr. J. E. Cunningham and Dr. K. Raj from SUN Microsystems for helpful discussions. Please note that the views, opinions, and/or findings contained in this article/presentation are those of the author/presenter and should not be interpreted as representing the official views or policies, either expressed or implied, of the Defense Advanced Research Projects Agency or the Department of Defense.

#117108 - $15.00 USD Received 11 Sep 2009; revised 12 Nov 2009; accepted 17 Nov 2009; published 24 Nov 2009